Open-source, partially 3D-printed, high-pressure (50 bar) liquid-nitrogen-cooled parahydrogen generator

Frowin Ellermann[1], Andrey Pravdivtsev[1], Jan-Bernd Hövener[1]

[1] Section for Biomedical Imaging, Molecular Imaging North Competence Center (MOIN CC), Department of Radiology and Neuroradiology, University Medical Center Schleswig-Holstein (UKSH), Kiel, 24118, Germany

Correspondence to: Frowin Ellermann (frowin.ellermann@rad.uni-kiel.de), Jan-Bernd Hövener (jan.hoevener@rad.uni-kiel.de)

Abstract. The signal of magnetic resonance imaging (MRI) can be enhanced by several orders of magnitude using hyperpolarization. In comparison to a broadly used Dynamic Nuclear Polarization (DNP) technique that is already used in clinical trials, the parahydrogen (pH$_2$) based hyperpolarization approaches are less cost-intensive, scalable and offer high throughput. However, a pH$_2$ generator is necessary. Available commercial pH$_2$ generators are relatively expensive (10,000 – 150,000 €). To facilitate the spread of pH$_2$ hyperpolarization studies, here, we provide the blueprints and 3D-models as open-source for a low-cost (<3,000 €) 50 bar liquid nitrogen pH$_2$ generator.

1 Introduction

Nuclear Magnetic Resonance (NMR), as well as Magnetic Resonance Imaging (MRI), are widely used in medical imaging and chemical analysis. Despite the great success of these techniques (Feyter et al., 2018; Lange et al., 2008; Watson et al., 2020), the low signal-to-noise ratio of NMR limits promising applications such as in vivo spectroscopy or imaging nuclei other than ^{1}H (Wilferth et al., 2020; Xu et al., 2008). The hyperpolarization of nuclear spins boosts the signal of selected molecules by orders of magnitude. This way, imaging of the lung or metabolism has become feasible (Beek et al., 2004; Kurhanewicz et al., 2011).

Among techniques, Parahydrogen And Synthesis Allows Dramatically Enhanced Nuclear Alignment (PASADENA) (Bowers and Weitekamp, 1986, 1987; Eisenschmid et al., 1987) has found application from catalysis research to metabolic imaging (Hövener et al., 2018; Kovtunov et al., 2018).

The production of parahydrogen (pH$_2$) is relatively easy: H$_2$ gas is flowing through a catalyst at cold temperatures; maximum para-enrichment of almost 100 % is achieved at about 25 K (Gamliel et al., 2010; Jeong et al., 2018; Kiryutin et al., 2017). To reach low temperatures, hence enrich pH$_2$, liquid cryogens (Buckenmaier et al., 2018; Jeong et al., 2018) or electric cryopumps (Feng et al., 2012) are used. Electronic setups were reported, e.g. for pressures up to 50 bar of ≈ 100 % pH$_2$ (Hövener et al.,

2013). Liquid nitrogen (lN_2)-based systems were described, however, often with limited description, low production rate and pressure.

Thus, in this contribution, we report a parahydrogen generator (PHG) based on lN_2 that operates at a pressure of up to 50 bar at a cost of less than 3000 €. The setup is easy to replicate as it is fully open-source (Ellermann, 2020b) and all parts are either off-the-shelf, 3D-printed or can be constructed easily. Besides, we introduce an automated pH_2 quantification method using a 1 T benchtop NMR and an Arduino-based process control.

Background In 1933 Werner Heisenberg received his Nobel Prize "for the creation of quantum mechanics, the application of which has, inter alia, led to the discovery of the allotropic forms of hydrogen" (NobelPrize.org, 2020). Allotropy is a property of substances to exist in several forms, in the same physical state. Two forms of hydrogen usually are referred to as nuclear spinisomers; they are parahydrogen (pH_2) and orthohydrogen (oH_2). Hydrogen is not the only compound that has stable or long-lived spinisomers at room temperature (rt), there are many examples: deuterium (Knopp et al., 2003), water (Kravchuk et al., 2011; Vermette et al., 2019) ,ethylene (Zhivonitko et al., 2013) and methyl groups (Meier et al., 2013). Although some molecules are not symmetric and cannot be extracted at room temperature, they possess long-lived spin states of minutes (Pileio et al., 2008) and hours (Stevanato et al., 2015).

The spin of hydrogen nuclei (of protons) is the origin of the two nuclear spinisomer forms of dihydrogen. Protons have spin-½, hence they are fermions. Fermions are particles that follow the Fermi-Dirac statistics, therefore the sign of the total wave function of H_2 has to change when two nuclei are exchanged. The spin space of two spin-½ consists of $\left(2 \cdot \frac{1}{2} + 1\right)^2 = 4$ states. They are three symmetric spin states: $|T_+\rangle = |\alpha\alpha\rangle$, $|T_0\rangle = (|\alpha\beta\rangle + |\beta\alpha\rangle)/\sqrt{2}$, $|T_-\rangle = |\beta\beta\rangle$ and one asymmetric nuclear spin state $|S\rangle = (|\alpha\beta\rangle - |\beta\alpha\rangle)/\sqrt{2}$ (Fig. 1). Here, conventionally $|\alpha\rangle$ and $|\beta\rangle$ states are nuclei spin states with the projection of spin on the Z axis ½ and -½, $|T_+\rangle$, $|T_0\rangle$ and $|T_-\rangle$ are triplet spin states of two spin-½ with a total spin of 1 and the projection on the Z axis +1, 0 and -1, and $|S\rangle$ is a singlet spin state of two spin ½ with a total spin of 0.

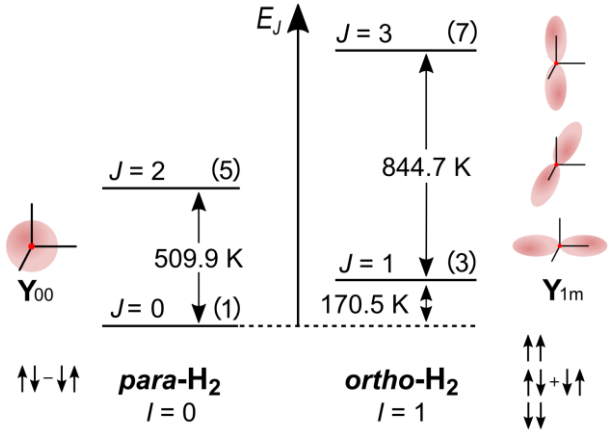

Figure 1: The rotational energy level diagram for isolated H_2. The angular distribution of the two lowest rotational states (Y_{00} corresponds to $J = 0$, and $Y_{1+1} \pm Y_{1-1}$ and Y_{10} corresponds to $J = 1$) and spin states of ortho and parahydrogen are indicated. The numbers in parenthesizes are the degeneracies of the state $2J + 1$. The energy of rotation spin states in units of K is equal to $E_J = J(J+1)\theta_R$ with $\theta_R =$ 87.6 K (Atkins and De Paula, 2006). The distance between two adjacent energy levels is $E_{J+1} - E_J = 2(J+1)\theta_R$. The figure was inspired by an illustration of I. F. Silvera (1980).

The rotational wave function after nuclei permutation does not change, because of the molecular symmetry, and is only multiplied by $(-1)^J$, with J being the rotational quantum number of the state. Hence, H_2 with a symmetric nuclear spin state (triplet states) can have only an asymmetric rotational state (J is odd); such H_2 is called *o*H_2. And vice versa, H_2 with an asymmetric nuclear spin state (singlet state) can have only symmetric rotation states (J is even); such H_2 is called *p*H_2.

The difference in the energy levels of two ground states of ortho ($J = 1$) and para ($J = 0$) hydrogen is $E_{J=1} - E_{J=0} = 2\theta_R \cong$ 175 K (Fig. 1) (Atkins and De Paula, 2006). Such a big energy gap allows a relatively simple way of spin-isomer enrichment: for H_2 the ground state is *p*H_2 and its population can be increased by cooling down the gas (Fig. 2) (M. Richardson et al., 2018). The ratio of the number of molecules of *p*H_2, n_{pH_2}, to *o*H_2, n_{oH_2}, in thermal equilibrium is given by the Boltzmann distribution of rotational energy levels:

$$\frac{n_{pH_2}}{n_{oH_2}} = \frac{\sum_{J=\text{even}\geq 0}(2J+1)\exp(-J(J+1)\theta_R/T)}{3\sum_{J=\text{odd}\geq 1}(2J+1)\exp(-J(J+1)\theta_R/T)}. \quad (1)$$

Since only two nuclear spinisomers states of H_2 exist, their fractions can be easily obtained: $f_{pH_2} = \frac{n_{pH_2}}{n_{pH_2}+n_{oH_2}} = \frac{1}{1+\frac{n_{oH_2}}{n_{pH_2}}}$ and $f_{oH_2} = \frac{1}{1+\frac{n_{pH_2}}{n_{oH_2}}}$. At room temperatures ($T \cong 298$ K) $n_{pH_2} : n_{oH_2}$ is close to 3: 1, at 77 K – the normal boiling point of nitrogen – the ratio is close to 1: 1, and at 25 K $f_{pH_2} \cong 98\%$ (Fig. 2).

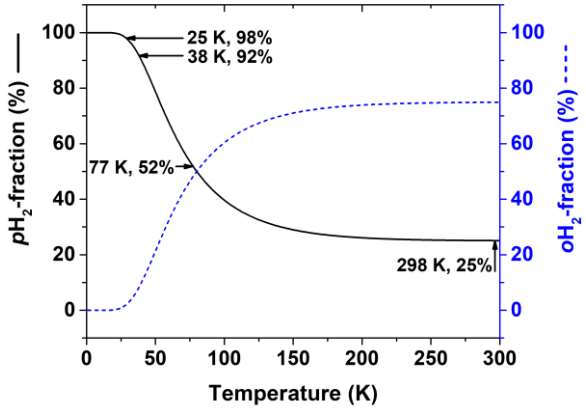

Figure 2: Thermal equilibrium fractions of *p*H_2 and *o*H_2 as a function of temperature calculated with Eq. 1 and $J = 6$. Four temperatures are marked: (1) 298 K – "room temperature", $f_{pH_2} \cong 25$ %, (2) 77 K – the boiling temperature of liquid nitrogen, $f_{pH_2} \cong$

52 %, (3) 38 K – medium conversion temperature of Bruker pH$_2$ generator, $f_{p\mathrm{H}_2} \cong 92$ %, (4) 25 K – conversion temperature of high-pressure PHG, $f_{p\mathrm{H}_2} \cong 98 \pm 2$ % (Hövener et al., 2013).

Technology review

pH$_2$ fraction, f_{pH_2}, of 90 % and above is produced by PHGs with single- or dual-stage cryostats run by Helium compressors. A single-stage cryostat was reported to operate at 36-40 K with a flow rate of 0.2 SLM (Standard Liter per Minute), 10 bar maximum delivery pressure, and $f_{p\mathrm{H}_2} \cong 85 - 92$ % (Bruker, Billerica, U.S.A.); dual-stage cryostats operate at temperatures below 25 K where $f_{p\mathrm{H}_2}$ reaches 100 % (note that the boiling point of H_2 is 21 K) (Haynes, 2011). All these PHGs were specifically designed with PHIP (ParaHydrogen Induced Polarization) in mind; meaning for a relatively low scale of production and in-lab use (not for the industry). These setups required some on-site assembling and were realized in different designs, e.g. with pulsed injection (Feng et al., 2012) or continuous flow (Hövener et al., 2013). The continuous flow setup was reported to operate at a conversion temperature of 25 K, a 4 SLM flow rate, a 50 bar maximum delivery pressure, and an experimentally obtained $f_{p\mathrm{H}_2} \cong 98 \pm 2$ % (Hövener et al., 2013).

These setups work reliably and don't require the supply of liquid cryogens. Disadvantages, however, include high initial investments (40.000 – 150.000 €), some maintenance of the He-compressor and cryostat (≈ 10.000 € every 25.000 h operational time), some site requirements (~4 kW cooling water, appropriate safety precautions) and operational cost in form of electricity (>4 kW electrical power) (Table 1).

A 100 % pH$_2$ enrichment, however, may not always be needed. 50 % pH$_2$ fraction provides already 1/3 of the maximum polarization at 1/10 of the costs (or less) (M. Richardson et al., 2018). To achieve f_{pH_2} of 50 %, 77 K, the temperature of lN_2, is sufficient. Indeed, lN_2-based PHGs are still used in many studies (Kiryutin et al., 2017; Meier et al., 2019). The design of such PHGs is generally simple - a catalyst chamber or tube immersed in lN_2. But just like cryostat-based PHGs, lN_2-based PHGs are continuously improving. As such, recent advances included a remarkable work, where 20 l lN_2 were sufficient to provide pH$_2$ continuously for 20 days (Jeong et al., 2018).

Interestingly, in various cases it was demonstrated that an increased flow rate and pressure of pH$_2$ can boost the signal of PHIP or Signal Amplification By Reversible Exchange (SABRE) (Adams et al., 2009; Rayner and Duckett, 2018) beyond the factor of 3 offered by PHGs with close to $f_{p\mathrm{H}_2} \cong 100\%$ (Colell et al., 2017; Rayner et al., 2017; Štěpánek et al., 2019; Truong et al., 2015).

Table 1: Performance comparison of several PHGs: (1) Bruker PHG 90, (2) dual-stage cryostats (DSC) (Hövener et al., 2013), (3) a pulsed PHG (Feng et al., 2012), (4) HyperSpin-PHG (Meier et al., 2019), (5) Automated PHG (Birchall et al., 2020), (6) He-dewar PHG (Du et al., 2020), (7) U-shape PHG (Kiryutin et al., 2017), (8) economical PHG (Jeong et al., 2018), (9) glass-trap PHG (Gamliel et al., 2010) and (10) in house designed and built PHG (this work). Given prices include all connectors, cylinders, and 19 % VAT. lN_2 stands for liquid nitrogen and "cc-He" for closed-cycle He compressor.

	Name	Operating temperature (K) [method]	f_{pH_2}(%)	Initial flow rate (SLM)	Max. pressure (bar)	Price (€)
1	Bruker PHG 90	36-40 [cc-He]	85-92	≤ 0.2	10	100,000–150,000
2	DSC (Hövener et al., 2013)	25 [cc-He]	98 ± 2	4	50	37,000
3	Pulsed PHG (Feng et al., 2012)	15 [cc-He]	98	0.9	20	N.A.
4	HyperSpin-PHG (Meier et al., 2019)	20-77 [cc-He]	N.A.[a]	N.A.	Min. 10	N.A.
5	Automated PHG (Birchall et al., 2020)	40 [cc-He]	~87	0.15	33.8	<25,000
6	He-dewar PHG (Du et al., 2020)	30 [He]	97.3 ± 1.9	~0.3	4.5	N.A.
7	U-shape PHG (Kiryutin et al., 2017)	77 [lN_2]	~50	0.36[b]	Min. 3	N.A.
8	Economical PHG (Jeong et al., 2018)	77 [lN_2]	~50	N.A.	N.A.	N.A.
9	Glass-trap PHG (Gamliel et al., 2010)	77 [lN_2]	46.3 ± 1.3	0.0025[c]	~1	N.A.
10	This work	77 [lN_2]	51.6 ± 0.9	2.0[d]	50[e]	2,988[f]

2 Methods

2.1 3D design of PHG

The principal scheme of a lN_2-based complete PHG consists of a H_2 gas supply, a generator and a pH_2 storage (Fig. 3). A model of the PHG was designed (Autodesk Inventor 2019, San Rafael, U.S.A.). Aluminium profiles and steel angles (30 mm, Bosch Rexroth, Stuttgart, Germany) were used to construct the chassis. Copper tubes (OD 6 mm, ID 4 mm, rated for 229 bar, R220, Landefeld, Kassel-Industriepark, Germany) and valves (Swagelok, Solon, U.S.A.) were mounted on the chassis using

[a] Depends on choice of coolant

[b] Estimated average flow (3.5 L volume filled to 3 bar in 90 min) calculated by us

[c] Estimated average flow (0.6 L volume filled to 1 bar in 240 min) calculated by us

[d] Highest average flow on filling 1 L bottle to 10 bar without sacrificing enrichment

[e] 50 bar pH_2 delivery was tested. Used parts allow pressure of at least 100 bar (safety margin)

[f] including H_2-gas sensor and excluding H_2 and N_2 bottles/regulators

3D-printed parts (Ultimaker PLA "Perlweiss" Filament, Ultimaker S5, Ultimaker Cura, Utrecht, Netherlands). A 2 L stainless steel dewar was placed in the chassis (DSS 2000, 2 L, KGW Isotherm, Karlsruhe, Germany). The same copper tubes were used to wind a coil with 5.4 turns and a diameter of 86 mm. About 1.5 ml granular Fe(OH)O (371254-50G, Sigma-Aldrich, St. Louis, U.S.A.) was filled into the coil. On both ends of the copper coil, cotton wool was pressed to keep the catalyst in place to protect the rest of the system from contaminations. The compressed wool insets have a length of 20 mm. Wool as a particulate filter was used before in another PHG (Du et al., 2020). During the six months of weekly use of our generator, there was no sign of a moving catalyst. All fittings, T-pieces, ball-valves, an overpressure-valve, flow regulators, a pressure gauge, and fast connectors (Swagelok, Solon, U.S.A.) were connected with the same copper tube. For the storage of pH$_2$, a 1 L cylinder made from aluminium was used (C1, A6341Q, Luxfer, Nottingham, UK). All parts were chosen to be rated for 100 bar or more to allow for a 100 % safety margin. A list of all parts is given in Appendix A. The models of the PHG, 3D-printing parts and experimental macros (experimental protocols) are available (Ellermann, 2020b).

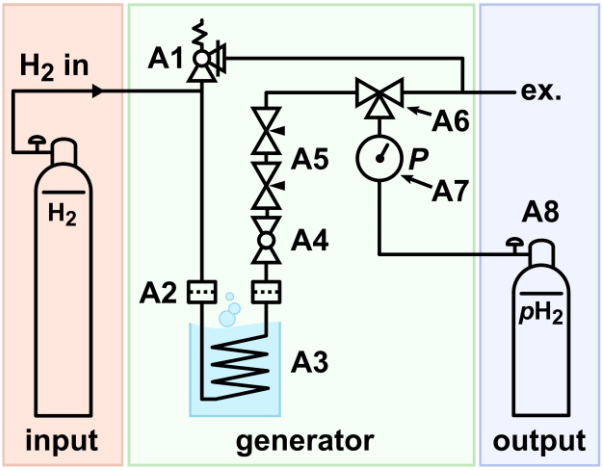

Figure 3: Schematic view of the PHG. H$_2$ gas is supplied via the inlet e.g. from a 50 L 200 bar cylinder. The gas flows through a filter (A2) into the ortho-para-conversion unit (A3) immersed in lN_2, where it is cooling down and thus getting enriched with the pH$_2$ component. The parahydrogen-enriched gas exits the ortho-para-conversion unit, warms up and passes another particle filter. The filters reduce the contamination of the setup with catalyst. A ball-valve (A4) is used to start or stop the gas flow. Two needle valves (A5) are used to control the flow rate. A 3-way-valve (A6) allows to fill or drain the storage cylinder. A 100 bar safety valve (A1) is connected to the system to relief a potential excess of pressure.

2.2 Safety concept

A crucial part of a PHG is the development of a safety concept which includes a detailed risk assessment and comprehensive operating manual. The handling of pressurized H$_2$ gas entails the risk of pressured gases, forming a potentially explosive mixture with air as well as hydrogen embrittlement (Beeson and Woods, 2003; National Aeronautics and Space Administration, 1997). To reduce these risks, the following safety requirements were set:

1. Safety by design
    a. Pressure ratings of parts
        i. All components, in contact with pressurized gas, are rated for minimum 100 bar
        ii. Mechanical pressure gauge
        iii. 100 bar safety valve for overpressure control
    b. Avoidance of formation of explosive H_2-air-mixture and potential ignition
        i. Reduction of H_2 in the system by minimizing the inner volume of the gas lines
        ii. No electrical components in the system
        iii. Avoidance of temperatures above flame point
        iv. Avoidance of inductive and static spark charges in the gas lines (due to conductive and groundable pipe material)
        v. High H_2 throughput and storage of pH_2 in small cylinder leads to a short operating time of PHG
    c. Easy maintenance due to the simple and open design concept
2. Safety by site and operation
    a. Strong ventilation in the installation site
    b. No public access
    c. Appropriate warning signs
    d. Usage by trained personnel according to manual only
    e. Use of safety goggles and safety gloves for the handling of lN_2
    f. H_2 sensor (for leakage alarm at 50 ppm H_2 level)
    g. Regular inspection and maintenance

2.3 Production protocol

All pH_2 batches were produced in the same manner (the indices in the brackets relate to in Fig. 3):

Preparation:

- Set initial state: Close valve A4, connect the generator with the output via A6 (“fill” position)
- Open and set supply of hydrogen to the appropriate pressure
- Connect the storage bottle A8 to the output
- Fill the dewar with lN_2 and close the lid to reduce evaporation
- Wait for 20 min and set the flow with the regulators A5

2. Flushing storage bottle:

- open valve A4 and wait until the pressure gauge shows 3 bar
- release gas from the storage cylinder by connecting the storage bottle to the exhaust via A6 (“venting position”)

- repeat the flushing steps three times

3. Production and storage of pH_2:

- Set valve A6 to "fill" position
- Wait until the gauge shows the desired pressure
- Close valve A4

4: Finishing production of pH_2:

- Close storage bottle (bottle valve)
- Set valve A6 to "vent" position to reduce pressure in the output line
- Disconnect storage bottle from the output (fast connect adapters keeps line closed)
- Set valve A6 to "close" position
- Close H_2 supply

2.4 Quantification

Flow quantification

We refrained from including a flow meter in the setup to keep it simple and robust. Instead, we used the time $t^{p,V}$ needed to fill a cylinder of a given volume V_0 to a given pressure p_{target} to measure the average flow rate f_{r} of the $p\text{H}_2$ production. The pressure p_{out} in the outlet of the PHG is increasing during production. To obtain Standard Liters per Minute (SLM) we used the following equation:

$$f_{\text{r}} = \frac{V_0}{t^{p,V}}\ [\text{SLM}] = \frac{p_{\text{out}} V_0 T_{\text{stand}}}{T_{\text{rt}} p_{\text{stand}}} \cdot \frac{1}{t^{p,V}} \quad (2)$$

where T_{rt} is the temperature of the quantification experiment (here: 22 °C) and "stand" stands for standard pressure and temperature values ($p_{\text{stand}} = 10^5$ pascals ≙ 1.0 bar, $T_{\text{stand}} = 273.15$ K) (Nič et al., 2009). The measurement of f_{r} is performed in a regime where p_{out} is linear as a function of time ($t^{p,V}$), hence it coincides with the initial flow rate that is usually reported.

Gas system

A medium-pressure 5 mm NMR tube (522-QPV-8, Wilmad-LabGlass, Vineland, U.S.A.) was used for the $p\text{H}_2$ quantification and a heavy wall 5 mm NMR tube (Wilmad-LabGlass, 522-PV-9) for experiments with Magnetic Field Cycling (MFC). Each of these NMR tubes was equipped with input and output gas lines (1/16" PolyTetraFluoroEthylene capillary (PTFE) with 0.023" inner diameter) by glueing them to the cap. The other end of these tubes was connected to a custom made valve system. The pressure in the system was set by changing the reducers of the respective gases and the back pressure valve in the gas system (P-785, P-787, Postnova). The inlet gas pressure was regulated to achieve a steady bubbling for the given backpressures of 2.8 bar and 6.9 bar. The valve system is controlled with an Arduino which was linked to the spectrometers software

synchronizing the gas supply, venting of the NMR tube, and data acquisition. Using this gas system we supplied to the NMR tube N_2 (99.999 %, Air Liquide), H_2 (99.999 %, Air Liquide) or pH_2.

pH_2 quantification protocol

The pH_2 quantification was performed according to a quantification protocol (schematically shown in Fig. 4).

A NMR tube is placed in a 1 T NMR spectrometer (benchtop, SpinSolve Carbon 43 MHz, Magritek, Aachen, Germany) and not moved during the experiment. To remove air and residual gases from the lines, the setup was flushed with the gas for 3 min at a 5 bar input pressure and a fully open exhaust. Afterwards, the exhaust line was closed and a 30 s delay was allowed to stabilize pressure and flow before the NMR acquisition was started. To ensure the constant pressure in the system, the gas supply was kept open during the NMR measurement. Because the NMR signal was not locked during the experiment, the H_2 resonance was moved to 0 ppm during post-processing for convenience.

All NMR spectra of gases were acquired with a standard excitation and acquisition of free induction decay pulse sequence (12.6 µs excitation pulse that corresponds to 90° flipping angle, 20 ms acquisition time, 50 kHz spectral width, 0.5 s repetition time, 100 transients for averaging, SpinSolve Expert v3.54, Magritek, Aachen, Germany). The spectra were subjected to 20 Hz exponential apodization and phase-correction. To remove background signals, a spectrum of N_2 was acquired also and subtracted from the rtH_2 (H_2 in thermal equilibrium at room temperature) and pH_2 spectra. After that, an automatic baseline correction (MNova v14.1.2, Santiago de Compostela, Spain) was applied to the phased spectrum. The spectral lines of rtH_2 and pH_2 were integrated within the borders of -15 ppm and +15 ppm giving $S(rtH_2)$ and $S(pH_2)$. Finally the fraction of pH_2 f_{pH_2} was calculated:

$$f_{pH_2} = \left(1 - \frac{3}{4}\frac{S(pH_2)}{S(rtH_2)}\right) \cdot 100\ \% \qquad (3)$$

Here it is taken into account, that only oH_2 contributes to the MR signal and $f_{pH_2} = \frac{1}{4}$ at room temperature (Green et al., 2012).

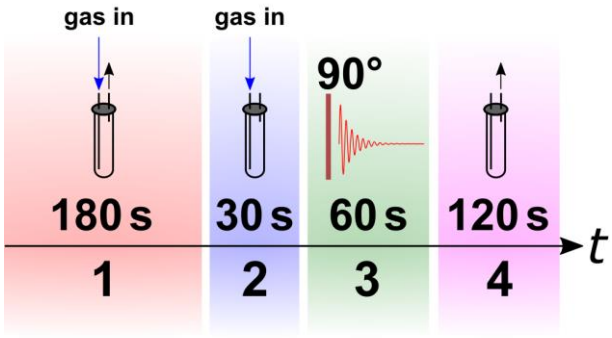

Figure 4: Scheme of pH_2 quantification protocol. The NMR tube is flushed with N_2, pH_2 or rtH_2 gas for 180 s before the exhaust is closed. A rest time of 30 s is allowed for the system to settle down. Finally, the NMR spectra are acquired, before the gas is released.

2.5 SABRE experiment

Sample preparation. The sample solution contained 3 mmol/L iridium N-heterocyclic carbene complex [Ir(COD)(IMes)Cl], where COD = 1,5-cyclooctadiene, Imes = 1,3-bis(2,4,6-trimethylphenyl) imidazol-2-ylidene (Cowley et al., 2011) and 26 mmol/L nicotinamide (CAS 98-92-0, Sigma-Aldrich) in methanol-d_4 99.8 % (Deutero GmbH). To activate the catalyst, H_2 was flushed through the sample at 6.9 bar for 5 minutes before the magnetic field cycling experiments begin.

Magnetic field cycling experiment. The NMR spectrometer was equipped with an in-house built MFC setup that will be described elsewhere. The shuttling time from the observation point to the sweet spot of the electromagnet was 0.2 seconds. The used electromagnet allowed a magnetic field variation in the range of -20 mT to +20 mT with a magnetic field homogeneity of 0.06 % in 2 cm. The same gas system as described above was used for the MFC SABRE experiments. The only modification was that a hollow optical fibre (Molex, part. num. 106815-0026, 250 µm internal diameter, 360 µm outer diameter) was glued to the end of the PTFE capillaries to reduce magnetic field distortions. All magnetic field-cycling SABRE experiments were carried out according to the protocol in Fig. 5.

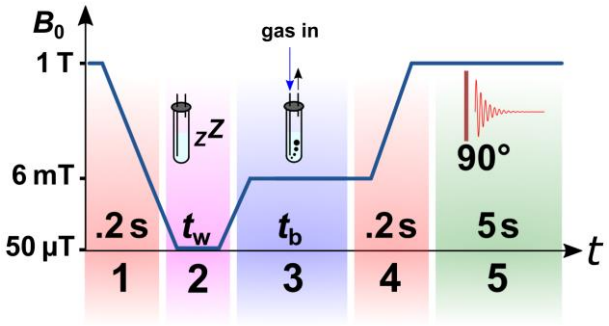

Figure 5: Scheme of ^{1}H magnetic field cycling SABRE experiment. *Stage 1*: shuttling of the sample to the polarization coil. *Stage 2:* relaxation of the sample at earth's magnetic field for t_w = 10 s. *Stage 3*: switching on the electromagnet with a magnetic field B_p = 6 mT and starting bubbling with pH$_2$ enriched gas at pressure P = 6.9 bar or 2.8 bar for t_b = 30 s. *Stage 4*: shuttling of the sample to the bore of the NMR spectrometer in 0.2 seconds and turning off the electromagnet. *Stage 5:* after 90° excitation, acquiring of the ^{1}H-NMR spectrum.

3 Results

3.1 PHG design

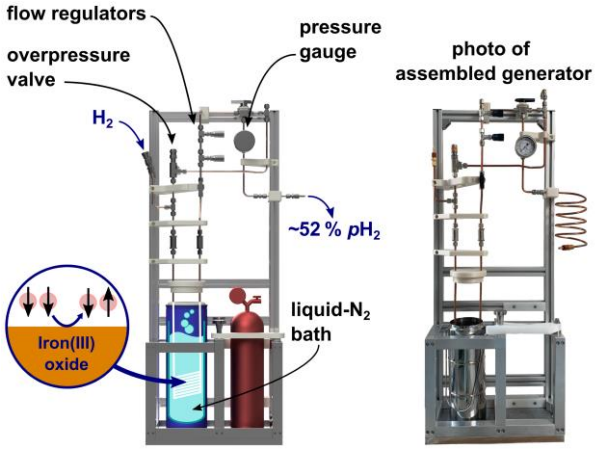

Figure 6: a) Rendering of the PHG (left) and a photo of the final build (right). The design of the PHG is open-source, simple and uses off-the-shelf as well as 3D-printed parts.

A PHG fulfilling the initial design requirements was successfully constructed (Fig. 6). Most parts were either commercially available, 3D printed or simple to construct on-site. The holders for the bottles and a bottom plate were the sole part prepared by a mechanical workshop. All parts were rated for more than 100 bars and no H_2 leaks were detected at 50 bars of H_2 using a H_2 detector (GasBadge Pro H2, Industrial Scientific, Pittsburgh, U.S.A.). Inspection and operation were facilitated by easy access and open construction design. The total cost was below 3,000 € (Appendix A).

We deliberately abstained from including a flow meter into the setup to keep the cost low and increase the robustness. Instead, we monitored the pressure p_{out} in the storage cylinder and calculated the flow rate (Fig. 7a). The expected increase in pressure and decrease in the flow rate of pH$_2$ was observed. The flow rate is an important parameter since it affects the amount of H_2 collisions with the catalyst in the ortho-para conversion unit (Fig. 3, A3) that enables fast para-ortho-conversion. A lN_2 based PHG can provide $f_{p\mathrm{H}_2} \cong 52$ % at maximum (Fig. 2,7b). If the flow rate is too fast, the gas will not have enough time to reach the ortho-para thermal equilibrium while passing through the unit. Hence the pH$_2$ fraction will be reduced.

Thus, to find optimal performance conditions of the PHG, we quantified $f_{p\mathrm{H}_2}$ as a function of the flow rate (Fig. 7c) set by the needle valves (Fig.3, A5). At the given settings of $p_{in} = 20$ bar and $p_{target} = 10$ bar, $f_{p\mathrm{H}_2} \approx 51.7$ % was found for a flow up to $f_r = 2$ SLM. For larger flow rates, the enrichment dropped significantly. Given this data, and to allow for some variation, we chose a standard operating flow of ~0.9 SLM. This flow rate was fast enough for a convenient pH$_2$ production. For example, l L of 49 bar pH$_2$ with $f_{p\mathrm{H}_2} = (51.7 \pm 0.8)$ % were produced in 29 min ($p_{in} = 49$ bar, initial flow rate of 2.9 SLM, Fig. 7a).

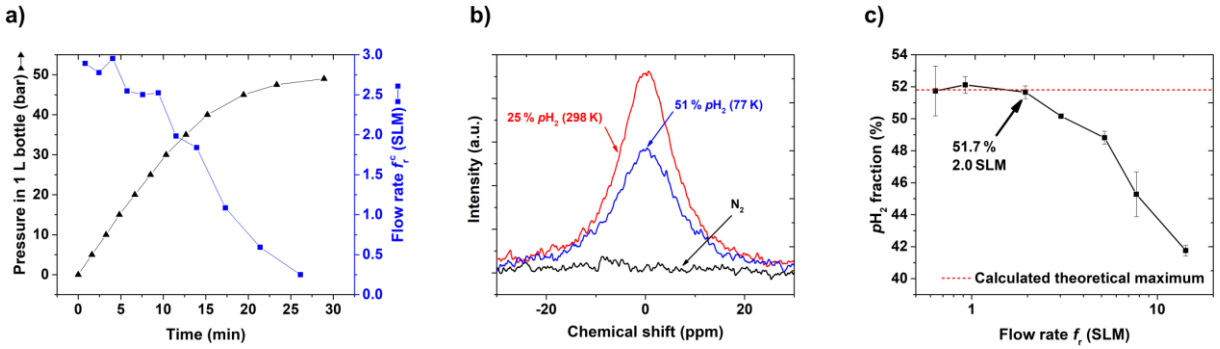

Figure 7: PHG operating parameters and NMR spectra: (a) Pressure p_{out} and calculated flow rate $f_r^c = p'_{out} \cdot \frac{V_0 T_{stand}}{T_{rt} P_{stand}}$ as a function of time for input pressure p_{in} = 50 bar and V_0 = 1 L, (b) ^{1}H NMR spectra of rtH$_2$, pH$_2$ and N$_2$ to quantify f_{pH_2}, and (c), f_{pH_2} as a function of f_r (eq. 3). For the latter, the para-enrichment was found to be constant up to a flow rate of f_r = 2 SLM (for p_{in} = 20 bar, p_{target} = 10 bar).

3.2 The precision of pH$_2$ production, quantification and lifetime

To test the reproducibility of the quantification method, f_{pH_2} of a single batch was quantified 5 times in a row (including venting, flushing, and filling of the tube). The average f_{pH_2} was found to be (51.5 ± 0.4) %, corresponding to a coefficient of variation (CV) of 0.7 % (Fig. 8).

To access the reproducibility of the entire production process, four pH$_2$ batches were produced on different days. An average f_{pH_2} of (51.6 ± 0.9) % was observed (CV = 1.7 %) (Fig. 8).

We also investigated f_{pH_2} as a function of the p_{in} pressure at a fixed flow rate: a batch was prepared for p_{in} equals 12 bar, 20 bar, 35 bar and 50 bar, p_{target} = 10 bar and a flow rate of 0.9 SLM. No pressure dependency could be observed. The obtained average of f_{pH_2} is (52.4 ± 0.8) %.

For evaluating the lifetime of pH$_2$ in the 2 L cylinder, a 10 bar pH$_2$ batch was produced (p_{in} = 20 bar, f_r = 0.9 SLM). Over 22 days, five samples were taken from the batch and f_{pH_2} was quantified. An exponential decay function was fitted to the data and yielded a constant of 35.5 ± 1.5 days (Fig. 9).

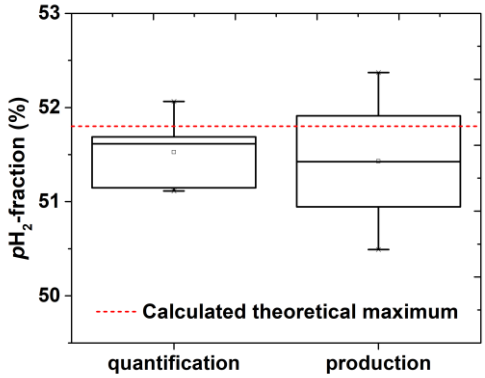

Figure 8: pH₂ quantification and production reproducibility chart. The left boxplot shows the precision of quantification method. The pH₂ quantification protocol was repeated five times with the same pH₂ batch. The obtained pH₂ fraction was (51.5 ± 0.4) % that gives us an impression of quantification precision. The right boxplot shows the reproducibility of the production. The production of pH₂ and quantification protocols were repeated once on four different days. The obtained pH₂ fraction here was (51.6 ± 0.9) %; the error value includes production and quantification errors. PHG parameters of pH₂ preparation: 20 bar inlet pressure, 10 bar final pressure in the storage cylinder and a 0.9 SLM average flow rate. All errors are given by the standard deviation.

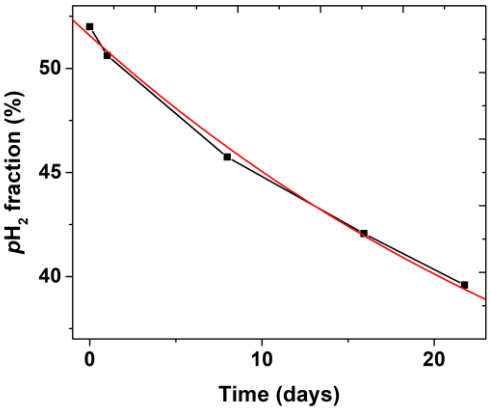

Figure 9: pH₂ lifetime in a 2 L aluminium cylinder. The data is fitted with the exponential decay function: $A_1 \cdot \exp(-t/\tau) + y_0$ with y_0 fixed to 25, A_1 = 26.6 ± 0.3 and a resulting relaxation decay time of τ = (35.5±1.5) days.

3.4 Application: ^{1}H-low-field SABRE at different pH₂ pressures

The presented setup was designed to allow for pressures up to 50 bar. High pressures are beneficial for hyperpolarization because the concentration of pH₂ in the solution increases with pressure. A low concentration of pH₂ is often the limiting factor

of the hyperpolarization yield (polarization level × concentration of polarized species). To demonstrate the effect, we polarized nicotine amide by SABRE and magnetic field-cycling (scheme at Fig. 5) at two different pH_2 pressures: 2.8 and 6.9 bar (Fig. 10). Strong polarization was observed on ^1H resonances of nicotine amide and hydrogen in solution and increased at higher pressure. A 2.5-fold increase in pressure yielded a 2.3-fold increase of nicotine amide polarization.

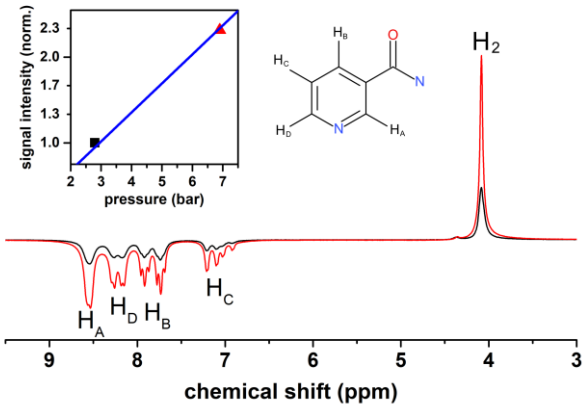

Figure 10: ^1H-SABRE spectra of nicotine amide and H_2 at 6.9 bar and 2.8 bar pH_2 pressure. (Insert) The signal intensity of nicotine amide vs. pressure with a linear fit (blue line). Nicotine amide structure is added for convenience.

4 Discussion

Design. The design of the presented PHG is simple and compact without compromising on performance and safety. The PHG is small and portable (although a heavy bottom plate was added for stability). Since there are no electrical components, it can be placed indoor as well as outdoor and does not require any electrical power supply. Note, electric components can be an ignition source which may lead to an explosion in case of a hydrogen leak.

For the framework, mostly, off-the-shelf parts were used. More complex geometries as e.g. holders for valves or gauges were 3D-printed. They have individual shapes and dimensions and manufacturing in a workshop might lead to high costs and long production lead times. 3D-printing turned out to be a versatile manufacturing method enabling fast prototyping, complex shapes, and low-cost for one-off productions. The design of the PHG and all 3D-models (STL-files, Standard Triangulation Language, and CAD-files, Computer-Aided Design) are provided enabling other groups to adjust the parts to their individual needs (Ellermann, 2020b).

Choosing a small 2 L dewar keeps the design compact and the running costs low since less than 2 L of liquid-nitrogen were required to prepare 1 L of pH_2 at 50 bar. In combination with a short cooling down time, the setup is perfectly suited for on-site pH_2 production in a hyperpolarization lab.

Costs. The final cost of the PHG incl. the hydrogen sensor is 2,988 € incl. VAT (19 %). If a hydrogen sensor is already available in the lab, the overall costs for the PHG can be pushed down to less than 2,500 € incl. VAT (19 %). A complete set including the PHG, a hydrogen sensor, hydrogen/nitrogen gas as well as a variety of essential tools costs about 3,700 € incl. VAT (19 %).

Safety. All parts which are in contact with pressurized gas are rated to at least 100 bar. However, we fixed the operation pressure to 50 bar to get a generous safety margin of 100 %. The risk for static and inductive spark charges in the gas line is low (Department of Labour of New Zealand, 1990). Nevertheless, the gas pipes can be grounded to prevent electrical charges on the parts which are in contact with H_2 gas.

The design of the PHG incorporates a gas path which also enables a safe ventilation of a storage bottle. The design and the choice of parts also consider potential handling errors. For example, the output connectors are closed for pressures up to 17 bar when they are disconnected, i.e. for the case that the storage bottle is disconnected. Thus, no contact between the air in the room and the hydrogen in the PHG occurred. Furthermore, we included a handheld hydrogen sensor that can measure hydrogen concentrations in the parts per million (ppm) regime. The sensor should be always turned on during operation and will indicate potential leakages of H_2 gas.

The setup includes low-temperature cryogens as liquid nitrogen. To prevent the spilling of liquid nitrogen, the dewar is restrained by the copper tubing inside and the surrounding metal frame. Moreover, a lid covers the liquid nitrogen bath that also reduces the evaporation rate of the cryogen. Since the flask only holds around 2 L of cryogen, the amount of liquid nitrogen that has to be handled is greatly reduced.

Note that PHG should be placed in a non-public lockable enclosure or room with sufficient ventilation and only instructed personnel should operate it.

Our presented safety concept is economical and practical without sacrificing any safety measures. Nevertheless, after setting up the PHG, it should be tested for leakage with inert gas or nitrogen. The part-list also contains a leak detection spray and the H_2 sensor.

Performance The enrichment achieved here, e.g. $f_{p\mathrm{H}_2}$ = 51.6 ± 0.9 % for p_{in} = 20 bar, f_{r} = 0.9 SLM, was close to the maximum of 51.8 % conditioned by the boiling point of lN_2, and somewhat higher than reported elsewhere $f_{p\mathrm{H}_2}$ = 50 % (Barskiy et al., 2016a, 2016b; Shchepin et al., 2016). Determining the enrichment as a function of flow allowed us to choose an optimal flow of 0.9 SLM for p_{in} = 20 bar: this rate is e.g. sufficient to fill 1 L bottles to 10 bar in 10 min. The central design criterium of high pressure was successfully met as 1 L of 49 bar $p\mathrm{H}_2$ were produced in 28 min (p_{in} = 50 bar). We demonstrated that an increase of $p\mathrm{H}_2$ pressure can give a proportional increase in polarization (Fig. 10). Obviously, this approach is limited as soon as the hyperpolarization yield is no longer determined by the availability of $p\mathrm{H}_2$ and cannot provide a polarization above 33% (Korchak et al., 2018).

***p*H₂ quantification and production reliability** The automatic quantification process features a CV of 0.7 %; the $p\mathrm{H}_2$ production and quantification together feature a CV of 1.7 % (Fig. 8). These results indicate, that the routine $p\mathrm{H}_2$ quality

control can be performed with a low-cost 1 T benchtop NMR spectrometer. The automatization certainly helps to make the process more reliable but is not necessary. Feng et al. used the same quantification approach and reported a precision of 1-3 % for quantification (2012). NMR is a convenient method for pH$_2$ quantification, but optical methods may be used, too (Parrott et al., 2019).

The lifetime in aluminium cylinder The relaxation time constant in aluminium tanks was found to be (63.7 ± 8.3) days by Feng et al. (2012) and ~120 days by Hövener et al., respectively (2013). We found here a shorter lifetime of (35.5 ± 1.5) days in our 2 L aluminium storage bottle. Note, that we did not perform any dedicated cleaning procedure for the pH$_2$ storage bottle. Still, the lifetime is sufficiently long to produce pH$_2$ once a week.

5 Conclusion

The presented PHG provides $f_{p\mathrm{H}_2} \approx 52$ % at a high pressure of 50 bar reliably (CV = 1.7 %) that provides about 1/3 of the polarization achieved with $f_{p\mathrm{H}_2} \approx 100$ %. Because the device provides high-pressure pH$_2$, however, this effect can be partially compensated in the PHIP/SABRE experiment. A new, automated quantification routine at 1 T benchtop NMR proved to be reliable and simple (CV = 0.7 %). The design of PHG is straightforward, easy to manufacture with openly available blueprints and at a cost of less than 3,000 €. The device may facilitate further research on the promising method of parahydrogen-based hyperpolarization.

6 Appendices

Table A1. Price list of all needed components for high-pressure PHG. Full list of items required for construction of portable liquid nitrogen parahydrogen generator (without cart) with 6 mm copper connection tubes. Here following format for item names is used: {Name [Company], (Specifications), Article number}. Given prices include 19 % VAT.

№	Name	Amount	Price, incl.VAT (Euro/unit)	Price, incl. VAT (Euro)
Gases and cylinders (148.00 €)				
1	Hydrogen cylinder [Airliquid], (Gas, ALPHAGAZ1, S10-1.8 m3), P0231S10R2A001	1	30.00	30.00
2	Nitrogen cylinder [Airliquid], (Gas, ALPHAGAZ1, S10-1.8 m3), P0271S10R2A001	1	40.00	40.00
3	Aluminium cylinder [Luxfer], (Cylinder, H_2 valve 28,8/21,8 LH), A6341Q	1	78.00	78.00

Regulators, gauges and valves (1578.92 €)				
4	Hydrogen cylinder pressure regulator [AirLiquide], (EUROJET 200/50, DIN 477-1, 6 mm tube outlet), Eurojet_125607	1	279.00	279.00
5	Nitrogen cylinder pressure regulator [Kayser], (in 200 bar, out 0-20 bar, DIN 477-1, 1/4" mm male ISO parallel thread), CK1302	1	128.00	128.00
6	Stainless Steel 1-Piece 40G Series Ball Valve [Swagelok], 0.6 Cv, 6 mm Tube Fitting	1	124.12	124.12
7	Stainless Steel High-Pressure Proportional Relief Valve [Swagelok], 6 mm Tube Fitting	1	253.83	253.83
8	Purple Spring for Proportional Relief Valve [Swagelok], 750 to 1500 psig (51.7 to 103 bar)	1	6.90	6.90
9	Stainless Steel 1-Piece 40G Series 3-Way Ball Valve [Swagelok], 0.90 Cv, 6 mm Tube Fitting	1	191.00	191.00
10	Stainless Steel Low Flow Metering Valve [Swagelok], 6 mm Tube Fitting, Vernier Handle	2	242.52	485.04
11	Gauge up to 100 bar [Swagelok], (6 mm tube fitting)	1	111.03	111.03
Tube and fittings (346.15 €)				
12	Copper tube, CUR6X1R Kupferrohr 6x1 mm, R 220, rolled good, soft, 1m [Landefeld]	5	11.29	56.45
13	Brass Instrumentation Quick Connect Stem with Valve [Swagelok], 0.2 Cv, 6 mm Tube Fitting	2	27.01	54.03
14	Brass Instrumentation Quick Connect Body [Swagelok], 0.2 Cv, 6 mm Bulkhead Tube Fitting	2	54.43	108.86
15	Stainless Steel Tube Fitting [Swagelok], Union, 6 mm Tube OD	1	17.91	17.91
16	Stainless Steel Swagelok Tube Fitting, Union Tee, 6 mm Tube OD	3	36.30	108.90
Rest (Catalyst, H_2 detector, Dewar,…, 1278.20 €)				
17	Iron(III) oxide [Merck] (catalyst grade, 30-50 mesh), 371254-50G	1	152.00	152.00
18	Hydrogen detector [Industrial Scientific], (GasBadge Pro H2, 0–2000 ppm), 18100060-C	1	499.00	499.00
19	Stainless steel liquid nitrogen Dewar flask [Isotherm], (DSS 2000, 2L, h=305, D=114), 2103	1	413.00	413.00

20	Stainless Steel In-Line Particulate Filter [Swagelok], 6 mm Tube Fitting, 90 Micron Pore Size	2	107.10	214.20
Gas exhaust line (59.80 €)				
21	Polyamid tube [AS-Drucklufttechnik GmbH], (6x3 mm, 1 m), PA 6X3 BLAU-25	5	1.36	6.80
22	Multiple plug connection [AS-Drucklufttechnik GmbH], (1x8mm, 4x6mm), IQSQ 8060	1	16.00	16.00
23	Reduction plug nipple [AS-Drucklufttechnik GmbH], (8mm to 6mm), IQSG 80H60	1	5.90	5.90
24	Check valve [AS-Drucklufttechnik GmbH], (6mm, 0.2 opening <0.2bar), HIQS 60	1	31.10	31.10
Tools (125.00 €)				
25	Clip [AS-Drucklufttechnik GmbH], (0 - 14 mm), SAS 14	1	9.2	9.20
26	Leak Detection Spray, [HM INDUSTRIESERVICE GMBH], 291-1252	1	15.1	15.10
27	Adjustable wrench RF 300 [Proxxon], (max 34 mm), 23994	1	26	26.00
28	Open ended wrench set	1	16.2	16.20
29	Pipe cutter [Landefeld], (3 - 30 mm), 4333097000773	1	57.5	57.50
30	PTFE thread seal tape	1	1.00	1.00
Frame parts (132.17 €)				
31	Rexroth profile 2 m each (2x 980 mm, 5x340 mm)	2	38.28	76.56
32	Rexroth *Nutenstein* M4/M5	14	1.12	15.66
33	Filament for 3D-printer: Ultimaker PLA *Perlweiß* 2,85 mm 750 g	1	39.95	39.95
34	In-house built metal parts (e.g. from university workshop)	0	0	0
35	Screws M4/M5	0	0	0
			Total price for the basic equipment incl. Hydrogen sensor, excl. VAT	2511.12*
			Total price for the basic equipment, incl. 19 % VAT	**2988.24***
			Total price for the complete set incl. tools and gases, excl. VAT	3082.55*
			Total price for the complete set incl. tools and gases, incl. 19 % VAT	3668.24*

***** Overall costs may vary due to change of prices, change of VAT rate, and due to costs which may arise for custom parts (e.g. material or labour costs from the facility's workshop)

7 Code availability

Software for automatic signal recording and gas control will be available from figshare.com (DOI: http://dx.doi.org/10.6084/m9.figshare.13176830) (Ellermann, 2020a) and via git (Ellermann, 2020b).

8 Data availability

All experimental data (SpinSolve ^{1}H NMR spectra of H_2) and blueprints for the PHG will be available from figshare.com (DOI: http://dx.doi.org/10.6084/m9.figshare.13176830) (Ellermann, 2020a). Additionally, all blueprints are also accessible via git (Ellermann, 2020b).

9 Team list

Frowin Ellermann (https://orcid.org/0000-0001-6446-6641)

Andrey N. Pravdivtsev (https://orcid.org/0000-0002-8763-617X)

Jan-Bernd Hövener (https://orcid.org/0000-0001-7255-7252)

10 Author contribution

Data curation, investigation, formal analysis, software development (here programming of macros), validation, visualization and writing of the original draft was done by FE. ANP and JBH contributed equally to conceptualization, supervision and reviewing the manuscript.

11 Competing interests

There are no competing interests to declare.

12 Disclaimer

13 Financial Support

We acknowledge support by the Emmy Noether Program “metabolic and molecular MR” (HO 4604/2-2), the research training circle “materials for brain” (GRK 2154/1-2019), DFG - RFBR grant (HO 4604/3-1, № 19-53-12013), the German Federal Ministry of Education and Research (BMBF) within the framework of the e:Med research and funding concept (01ZX1915C), Cluster of Excellence “precision medicine in inflammation” (PMI 1267). Kiel University and the Medical Faculty are

acknowledged for supporting the Molecular Imaging North Competence Center (MOIN CC) as a core facility for imaging in vivo. MOIN CC was founded by a grant from the European Regional Development Fund (ERDF) and the Zukunftsprogramm Wirtschaft of Schleswig-Holstein (Project no. 122-09-053).

14. References

Adams, R. W., Aguilar, J. A., Atkinson, K. D., Cowley, M. J., Elliott, P. I. P., Duckett, S. B., Green, G. G. R., Khazal, I. G., López-Serrano, J. and Williamson, D. C.: Reversible Interactions with para-Hydrogen Enhance NMR Sensitivity by Polarization Transfer, Science, 323(5922), 1708–1711, doi:10.1126/science.1168877, 2009.

Atkins, P. W. and De Paula, J.: Physical chemistry, Oxford University Press, Oxford; New York., 2006.

Barskiy, D. A., Salnikov, O. G., Shchepin, R. V., Feldman, M. A., Coffey, A. M., Kovtunov, K. V., Koptyug, I. V. and Chekmenev, E. Y.: NMR SLIC Sensing of Hydrogenation Reactions Using Parahydrogen in Low Magnetic Fields, J. Phys. Chem. C, 120(51), 29098–29106, doi:10.1021/acs.jpcc.6b07555, 2016a.

Barskiy, D. A., Shchepin, R. V., Coffey, A. M., Theis, T., Warren, W. S., Goodson, B. M. and Chekmenev, E. Y.: Over 20% 15N Hyperpolarization in Under One Minute for Metronidazole, an Antibiotic and Hypoxia Probe, J. Am. Chem. Soc., 138(26), 8080–8083, doi:10.1021/jacs.6b04784, 2016b.

Beek, E. J. R. van, Wild, J. M., Kauczor, H.-U., Schreiber, W., Mugler, J. P. and Lange, E. E. de: Functional MRI of the lung using hyperpolarized 3-helium gas, Journal of Magnetic Resonance Imaging, 20(4), 540–554, doi:10.1002/jmri.20154, 2004.

Beeson, H. and Woods, S.: Guide for Hydrogen Hazards Analysis on Components and Systems, Components and Systems, 40, 2003.

Birchall, J. R., Coffey, A. M., Goodson, B. M. and Chekmenev, E. Y.: High-Pressure Clinical-Scale 87% Parahydrogen Generator, Anal. Chem., doi:10.1021/acs.analchem.0c03358, 2020.

Bowers, C. R. and Weitekamp, D. P.: Transformation of Symmetrization Order to Nuclear-Spin Magnetization by Chemical Reaction and Nuclear Magnetic Resonance, Phys. Rev. Lett., 57(21), 2645–2648, doi:10.1103/PhysRevLett.57.2645, 1986.

Bowers, C. R. and Weitekamp, D. P.: Parahydrogen and synthesis allow dramatically enhanced nuclear alignment, J. Am. Chem. Soc., 109(18), 5541–5542, doi:10.1021/ja00252a049, 1987.

Buckenmaier, K., Rudolph, M., Fehling, P., Steffen, T., Back, C., Bernard, R., Pohmann, R., Bernarding, J., Kleiner, R., Koelle, D., Plaumann, M. and Scheffler, K.: Mutual benefit achieved by combining ultralow-field magnetic resonance and hyperpolarizing techniques, Review of Scientific Instruments, 89(12), 125103, doi:10.1063/1.5043369, 2018.

Colell, J. F. P., Logan, A. W. J., Zhou, Z., Shchepin, R. V., Barskiy, D. A., Ortiz, G. X., Wang, Q., Malcolmson, S. J., Chekmenev, E. Y., Warren, W. S. and Theis, T.: Generalizing, Extending, and Maximizing Nitrogen-15 Hyperpolarization Induced by Parahydrogen in Reversible Exchange, J. Phys. Chem. C, 121(12), 6626–6634, doi:10.1021/acs.jpcc.6b12097, 2017.

Cowley, M. J., Adams, R. W., Atkinson, K. D., Cockett, M. C. R., Duckett, S. B., Green, G. G. R., Lohman, J. A. B., Kerssebaum, R., Kilgour, D. and Mewis, R. E.: Iridium N-Heterocyclic Carbene Complexes as Efficient Catalysts for Magnetization Transfer from para-Hydrogen, J. Am. Chem. Soc., 133(16), 6134–6137, doi:10.1021/ja200299u, 2011.

Department of Labour of New Zealand: Guidelines for the CONTROL OF STATICELECTRICITY ININDUSTRY, 1990.

Du, Y., Zhou, R., Ferrer, M.-J., Chen, M., Graham, J., Malphurs, B., Labbe, G., Huang, W. and Bowers, C. R.: An Inexpensive Apparatus for up to 97% Continuous-Flow Parahydrogen Enrichment Using Liquid Helium, Journal of Magnetic Resonance, 106869, doi:10.1016/j.jmr.2020.106869, 2020.

Eisenschmid, T. C., Kirss, R. U., Deutsch, P. P., Hommeltoft, S. I., Eisenberg, R., Bargon, J., Lawler, R. G. and Balch, A. L.: Para hydrogen induced polarization in hydrogenation reactions, J. Am. Chem. Soc., 109(26), 8089–8091, doi:10.1021/ja00260a026, 1987.

Ellermann, F.: figshare: opensource-liquid-N2-based pH2 Generator, opensource-liquid-N2-based pH2 Generator [online] Available from: http://dx.doi.org/10.6084/m9.figshare.13176830, 2020a.

Ellermann, F.: git: opensource-liquid-N2-based pH2 Generator, opensource-liquid-N2-based pH2 Generator [online] Available from: https://gitlab.tardis.rad.uni-kiel.de/fellermann/opensource-liquid-n2-based-ph2-generator, 2020b.

Feng, B., Coffey, A. M., Colon, R. D., Chekmenev, E. Y. and Waddell, K. W.: A pulsed injection parahydrogen generator and techniques for quantifying enrichment, J. Magn. Reson., 214, 258–262, doi:10.1016/j.jmr.2011.11.015, 2012.

Feyter, H. M. D., Behar, K. L., Corbin, Z. A., Fulbright, R. K., Brown, P. B., McIntyre, S., Nixon, T. W., Rothman, D. L. and Graaf, R. A. de: Deuterium metabolic imaging (DMI) for MRI-based 3D mapping of metabolism in vivo, Science Advances, 4(8), eaat7314, doi:10.1126/sciadv.aat7314, 2018.

Gamliel, A., Allouche-Arnon, H., Nalbandian, R., Barzilay, C. M., Gomori, J. M. and Katz-Brull, R.: An Apparatus for Production of Isotopically and Spin-Enriched Hydrogen for Induced Polarization Studies, Appl Magn Reson, 39(4), 329–345, doi:10.1007/s00723-010-0161-9, 2010.

Green, R. A., Adams, R. W., Duckett, S. B., Mewis, R. E., Williamson, D. C. and Green, G. G. R.: The theory and practice of hyperpolarization in magnetic resonance using parahydrogen, Prog. Nucl. Magn. Reson. Spectrosc., 67(Supplement C), 1–48, doi:10.1016/j.pnmrs.2012.03.001, 2012.

Haynes, W. M.: CRC Handbook of Chemistry and Physics, in CRC Handbook of Chemistry and Physics, p. 4.121–4.123, CRC Press, New York, NY., 2011.

Hövener, J.-B., Bär, S., Leupold, J., Jenne, K., Leibfritz, D., Hennig, J., Duckett, S. B. and von Elverfeldt, D.: A continuous-flow, high-throughput, high-pressure parahydrogen converter for hyperpolarization in a clinical setting, NMR Biomed., 26(2), 124–131, doi:10.1002/nbm.2827, 2013.

Hövener, J.-B., Pravdivtsev, A. N., Kidd, B., Bowers, C. R., Glöggler, S., Kovtunov, K. V., Plaumann, M., Katz-Brull, R., Buckenmaier, K., Jerschow, A., Reineri, F., Theis, T., Shchepin, R. V., Wagner, S., Bhattacharya, P., Zacharias, N. M. and Chekmenev, E. Y.: Parahydrogen-Based Hyperpolarization for Biomedicine, Angewandte Chemie International Edition, 57(35), 11140–11162, doi:10.1002/anie.201711842, 2018.

Jeong, K., Min, S., Chae, H. and Namgoong, S. K.: Detecting low concentrations of unsaturated C-C bonds by parahydrogen-induced polarization using an efficient home-built parahydrogen generator, Magnetic Resonance in Chemistry, 56(11), 1089–1093, doi:10.1002/mrc.4756, 2018.

Kiryutin, A. S., Sauer, G., Hadjiali, S., Yurkovskaya, A. V., Breitzke, H. and Buntkowsky, G.: A highly versatile automatized setup for quantitative measurements of PHIP enhancements, J. Magn. Reson., 285(Supplement C), 26–36, doi:10.1016/j.jmr.2017.10.007, 2017.

Knopp, G., Kirch, K., Beaud, P., Mishima, K., Spitzer, H., Radi, P., Tulej, M. and Gerber, T.: Determination of the ortho-/para deuterium concentration ratio with femtosecond CARS, Journal of Raman Spectroscopy, 34(12), 989–993, doi:10.1002/jrs.1091, 2003.

Korchak, S., Mamone, S. and Glöggler, S.: Over 50 % 1H and 13C Polarization for Generating Hyperpolarized Metabolites—A para-Hydrogen Approach, ChemistryOpen, 7(9), 672–676, doi:10.1002/open.201800086, 2018.

Kovtunov, K. V., Pokochueva, E. V., Salnikov, O. G., Cousin, S. F., Kurzbach, D., Vuichoud, B., Jannin, S., Chekmenev, E. Y., Goodson, B. M., Barskiy, D. A. and Koptyug, I. V.: Hyperpolarized NMR Spectroscopy: d-DNP, PHIP, and SABRE Techniques, Chemistry – An Asian Journal, 13(15), 1857–1871, doi:10.1002/asia.201800551, 2018.

Kravchuk, T., Reznikov, M., Tichonov, P., Avidor, N., Meir, Y., Bekkerman, A. and Alexandrowicz, G.: A Magnetically Focused Molecular Beam of Ortho-Water, Science, 331(6015), 319–321, doi:10.1126/science.1200433, 2011.

Kurhanewicz, J., Vigneron, D. B., Brindle, K., Chekmenev, E. Y., Comment, A., Cunningham, C. H., DeBerardinis, R. J., Green, G. G., Leach, M. O., Rajan, S. S., Rizi, R. R., Ross, B. D., Warren, W. S. and Malloy, C. R.: Analysis of Cancer Metabolism by Imaging Hyperpolarized Nuclei: Prospects for Translation to Clinical Research, Neoplasia, 13(2), 81–97, doi:10.1593/neo.101102, 2011.

Lange, O. F., Lakomek, N.-A., Farès, C., Schröder, G. F., Walter, K. F. A., Becker, S., Meiler, J., Grubmüller, H., Griesinger, C. and Groot, B. L. de: Recognition Dynamics Up to Microseconds Revealed from an RDC-Derived Ubiquitin Ensemble in Solution, Science, 320(5882), 1471–1475, doi:10.1126/science.1157092, 2008.

Meier, B., Dumez, J.-N., Stevanato, G., Hill-Cousins, J. T., Roy, S. S., Håkansson, P., Mamone, S., Brown, R. C. D., Pileio, G. and Levitt, M. H.: Long-Lived Nuclear Spin States in Methyl Groups and Quantum-Rotor-Induced Polarization, J. Am. Chem. Soc., 135(50), 18746–18749, doi:10.1021/ja410432f, 2013.

Meier, B., Kouril, K. and Kourilova, H.: Para-Hydrogen Generator. Low-cost para-hydrogen for anyone, [online] Available from: http://www.hyperspin.biz/#php, 2019.

M. Richardson, P., O. John, R., J. Parrott, A., J. Rayner, P., Iali, W., Nordon, A., E. Halse, M. and B. Duckett, S.: Quantification of hyperpolarisation efficiency in SABRE and SABRE-Relay enhanced NMR spectroscopy, Phys. Chem. Chem. Phys., doi:10.1039/C8CP05473H, 2018.

National Aeronautics and Space Administration: Safety Standard for Hydrogen and Hydrogen Systems, 1997.

Nič, M., Jirát, J., Košata, B., Jenkins, A. and McNaught, A., Eds.: standard conditions for gases, in IUPAC Compendium of Chemical Terminology, IUPAC, Research Triagle Park, NC., 2009.

NobelPrize.org: The Nobel Prize in Physics 1932, NobelPrize.org [online] Available from: https://www.nobelprize.org/prizes/physics/1932/summary/ (Accessed 16 October 2020), 2020.

Parrott, A. J., Dallin, P., Andrews, J., Richardson, P. M., Semenova, O., Halse, M. E., Duckett, S. B. and Nordon, A.: Quantitative In Situ Monitoring of Parahydrogen Fraction Using Raman Spectroscopy, Appl Spectrosc, 73(1), 88–97, doi:10.1177/0003702818798644, 2019.

Pileio, G., Carravetta, M., Hughes, E. and Levitt, M. H.: The long-lived nuclear singlet state of 15N-nitrous oxide in solution, J Am Chem Soc, 130(38), 12582–12583, doi:10.1021/ja803601d, 2008.

Rayner, P. J. and Duckett, S. B.: Signal Amplification by Reversible Exchange (SABRE): From Discovery to Diagnosis, Angewandte Chemie International Edition, 57(23), 6742–6753, doi:10.1002/anie.201710406, 2018.

Rayner, P. J., Burns, M. J., Olaru, A. M., Norcott, P., Fekete, M., Green, G. G. R., Highton, L. A. R., Mewis, R. E. and Duckett, S. B.: Delivering strong 1H nuclear hyperpolarization levels and long magnetic lifetimes through signal amplification by reversible exchange, PNAS, 201620457, doi:10.1073/pnas.1620457114, 2017.

Shchepin, R. V., Barskiy, D. A., Coffey, A. M., Theis, T., Shi, F., Warren, W. S., Goodson, B. M. and Chekmenev, E. Y.: 15N Hyperpolarization of Imidazole-15N2 for Magnetic Resonance pH Sensing via SABRE-SHEATH, ACS Sens., 1(6), 640–644, doi:10.1021/acssensors.6b00231, 2016.

Silvera, I. F.: The solid molecular hydrogens in the condensed phase: Fundamentals and static properties, Rev. Mod. Phys., 52(2), 393–452, doi:10.1103/RevModPhys.52.393, 1980.

Štěpánek, P., Sanchez-Perez, C., Telkki, V.-V., Zhivonitko, V. V. and Kantola, A. M.: High-throughput continuous-flow system for SABRE hyperpolarization, Journal of Magnetic Resonance, 300, 8–17, doi:10.1016/j.jmr.2019.01.003, 2019.

Stevanato, G., Hill-Cousins, J. T., Håkansson, P., Roy, S. S., Brown, L. J., Brown, R. C. D., Pileio, G. and Levitt, M. H.: A Nuclear Singlet Lifetime of More than One Hour in Room-Temperature Solution, Angew. Chem. Int. Ed., 54(12), 3740–3743, doi:10.1002/anie.201411978, 2015.

Truong, M. L., Theis, T., Coffey, A. M., Shchepin, R. V., Waddell, K. W., Shi, F., Goodson, B. M., Warren, W. S. and Chekmenev, E. Y.: 15N Hyperpolarization by Reversible Exchange Using SABRE-SHEATH, J. Phys. Chem. C, 119(16), 8786–8797, doi:10.1021/acs.jpcc.5b01799, 2015.

Vermette, J., Braud, I., Turgeon, P.-A., Alexandrowicz, G. and Ayotte, P.: Quantum State-Resolved Characterization of a Magnetically Focused Beam of ortho-H2O, J. Phys. Chem. A, 123(42), 9234–9239, doi:10.1021/acs.jpca.9b04294, 2019.

Watson, W. D., Miller, J. J. J., Lewis, A., Neubauer, S., Tyler, D., Rider, O. J. and Valkovič, L.: Use of cardiac magnetic resonance to detect changes in metabolism in heart failure, Cardiovascular Diagnosis and Therapy, 10(3), 583-597–597, doi:10.21037/cdt.2019.12.13, 2020.

Wilferth, T., Gast, L. V., Lachner, S., Behl, N. G. R., Schmidt, M., Dörfler, A., Uder, M. and Nagel, A. M.: X-Nuclei MRI on a 7T MAGNETOM Terra: Initial Experiences, MAGNETOM Flash, (76), 7, 2020.

Xu, V., Chan, H., Lin, A., Sailasuta, N., Valencerina, S., Tran, T., Hovener, J. and Ross, B.: MR Spectroscopy in Diagnosis and Neurological Decision-Making, Semin Neurol, 28(04), 407–422, doi:10.1055/s-0028-1083685, 2008.

Zhivonitko, V. V., Kovtunov, K. V., Chapovsky, P. L. and Koptyug, I. V.: Nuclear Spin Isomers of Ethylene: Enrichment by Chemical Synthesis and Application for NMR Signal Enhancement, Angew. Chem. Int. Ed., 52(50), 13251–13255, doi:10.1002/anie.201307389, 2013.